Pergamon

Int. J. Solids Structures Vol. 31, No. 18, pp. 2537–2563, 1994
Elsevier Science Ltd
Printed in Great Britain
0020–7683/94 $7.00 + .00

AN EVALUATION OF ANALYTICAL AND NUMERICAL SOLUTIONS TO THE SINGLE-LAP JOINT

M. Y. TSAI and J. MORTON
Department of Engineering Science and Mechanics, Virginia Polytechnic Institute and State University, Blacksburg, VA 24061-0219, U.S.A.

(*Received* 9 *October* 1992; *in revised form* 6 *May* 1993)

Abstract—The mechanics of a single-lap joint subjected to tensile loading are investigated. Theoretical solutions, including the classic Goland and Reissner solution, are reviewed and examined in detail. It is observed that, despite the considerable efforts of a large number of researchers over a period of half a century, controversy and unresolved issues remain. Limitations related to theoretical treatments are identified and suggested improvements proposed.

A two-dimensional geometrically nonlinear finite element analysis is performed to provide comparisons with the theoretical analyses. The discrepancies and controversies in the theories are resolved through detailed studies of the mechanics and validated through numerical analyses, and through a clarification of the definition of long and short joints. Modifications and corrections to the theories are suggested for practical application to lap joint analysis and design.

INTRODUCTION

The single-lap joint is one of the most commonly used bonding configurations. Due to its combined characteristics of simplicity and efficiency, the single-lap joint has been adopted as a standard mechanical test method for determining the shear strength (ASTM D1002-72) and modulus (ASTM D3983-81) properties of adhesives. In addition, it has also gained the attention of aerospace, automotive, as well as the wood and plastics industries for structural joint evaluation.

Whether for determining the material properties of adhesives or for structural bonding applications, the single-lap joint must be analysed in detail to provide an understanding of the stress distributions not only in the adhesive layer, but also in the joint adherends, under mechanical loading and under the relevant environmental conditions (such as temperature, moisture, etc.). The stress analysis of the single-lap joint has undergone continuous development and refinement for more than five decades. The earliest analysis developed by Volkersen (1938) was a simple shear lag model based on the assumptions of a perfectly rigid adherend with only shear deformation in the adhesive layer. Later, Goland and Reissner (1944) developed a cylindrically bent-plate analysis in which the major steps were: to introduce the effects of a joint edge moment, resulting from the eccentricity of the loading path, on the stress distributions in the adherends and the adhesive; to formulate the adhesive stress distributions in terms of the geometrical and material parameters of the adherend and adhesive; to demonstrate the critical role of the transverse normal (peel) stress component at (or near) the free end of the adhesive layer. Hart-Smith (1973) proposed an improved model which removes the lumped overlap (assumed in the Goland and Reissner analysis) restriction by treating the adherends as beams on an elastic foundation, and provided stress solutions for linear elastic and elastic–plastic adhesives. Recently, Oplinger (1991) developed a layered beam analysis, which included treatment of large deflection of the joint overlap.

Several researchers have proposed two-dimensional analytical solutions, which were focused on the joint overlap, to ensure that the stress-free boundary conditions would be satisfied at the free end. For example, Allman (1977) used a minimum strain energy, with given bending, stretching and shearing at the end of the overlap and assuming that the longitudinal normal stress was zero, the shear stress constant and transverse normal stress linearly distributed across the thickness of the adhesive. Chen and Cheng (1983) employed the variational principle of complementary energy with similar boundary conditions and assumptions to those of Allman.

The finite element method has been used by Wooley and Carver (1971) who conducted a geometrically linear analysis and performed extensive parametric studies. Adams and Peppiatt (1974), and Crocombe and Adams (1981) performed two-dimensional linear finite element analyses of the single-lap joint with a spew fillet. Harris and Adams (1984) performed a nonlinear finite element stress analysis focused on the prediction of the strength for a single-lap joint with a spew fillet, with linear elastic and elastic–plastic material properties of the adhesives.

The critical feature of the single-lap joint is the eccentric loading path, which results in large deflections of the outer adherend and the overlap, and the joint edge moment (M_o) at the end of the overlap. Goland and Reissner (1944) showed that M_o plays the dominant role in the development of the stress distributions in both the adherends and the adhesive layers. The magnitude of M_o depends on the geometry, material properties and the applied load, and cannot be predicted from one-dimensional beam theory without including large deflection effects or from two-dimensional elasticity without including geometric nonlinearity. The complexity arising from the geometric nonlinearity has been eliminated by applying M_o, the edge shear force (V_o) and the stretching load (T) as force boundary conditions (see Fig. 1) in two-dimensional linear stress analyses of the joint overlap. For example, Ojalvo and Eidinoff (1978) used Hart-Smith's M_o formulation, while Chen and Cheng (1983), and Crocombe and Adams (1981) adopted Goland and Reissner's formulation. Thus an accurate evaluation of M_o is essential.

Since the joint edge moment is such a crucial parameter, it is instructive to compare the first formulation postulated by Goland and Reissner (1944) to the modified treatment

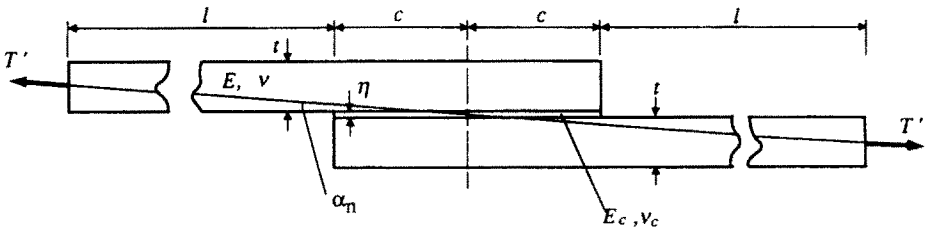

(a)

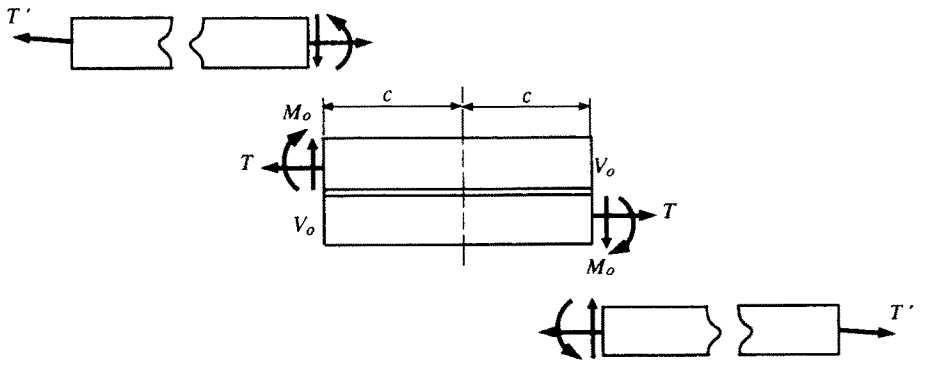

(b)

Fig. 1. Schematic representation of a single-lap joint: (a) geometric and material parameters; (b) free-body diagrams under loading.

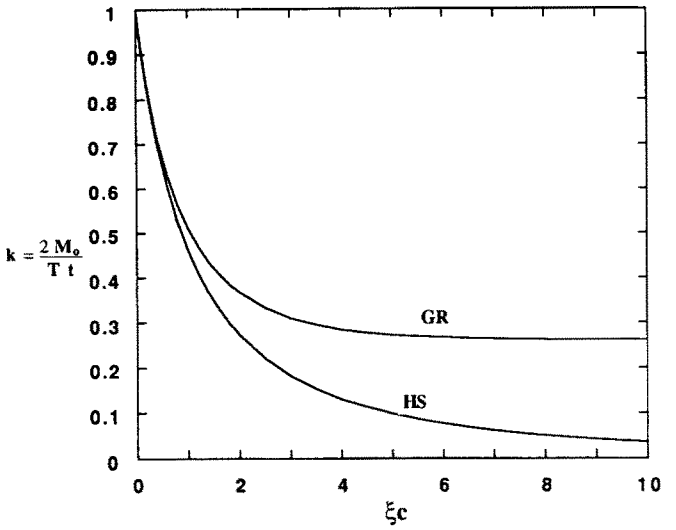

Fig. 2. The normalized edge moment k vs ξc for the original Goland and Reissner (GR) and Hart-Smith (HS) analyses for $\eta = 0$.

of Hart-Smith (1973). Both approaches lead to the rather different values of M_o shown in Fig. 2. The above formulations are widely cited by other researchers (Adams, Cheng, Allman, Ojalvo, Oplinger, etc.). However, there are conflicts, and the accuracy of these formulations is still in question. The objectives of the present study are to evaluate the theoretical models, to clarify the limitations of the models, to resolve the apparent conflicts, and to present reliable stress distributions in the adhesive layer.

THEORETICAL FORMULATIONS

The geometrical and material parameters of the single-lap joint are shown in Fig. 1(a), in which α_n represents a force-eccentricity angle, l the length of the outer adherend, $2c$ the length of the overlap, t the thickness of the adherend, and η the thickness of the adhesive layer. The elastic modulus and Poisson's ratio are E and v, respectively, for the adherends, and E_c and v_c for the adhesive. When the single-lap joint is subjected to a stretching load, T', the free-body diagrams shown in Fig. 1(b) illustrate the presence of the joint edge moment, M_o, the joint edge shear force, V_o, and the longitudinal force, T per unit width, at the ends of the overlap. Since $\alpha_n \ll 1$ (usually $\alpha_n < 0.1$), the relationship between T and T' can be written as:

$$T = T' \cos \alpha_n \cong T' = pt, \tag{1}$$

where p is an applied average stress. The force system acting on the overlap portion in Fig. 1(b), must satisfy the self-equilibrium condition,

$$V_o = \left[\frac{T}{2}(t+\eta) - M_o\right] \Big/ c. \tag{2}$$

Goland and Reissner (1944)

This classic analysis of the single-lap joint can be divided into three parts: part I, the determination of the edge loads; part II, the stress analysis of the overlap for a relatively inflexible adhesive; part III, the stress analysis of the overlap for a relatively flexible adhesive. In part I, it was assumed that the adhesive layer was thin compared to the thickness of the adherend ($\eta \ll t$) so that the presence of the adhesive layer was neglected, and η and E_c are eliminated from the formulation. The analyses took into account the

effects of large deflections for the outer adherend and the joint overlap. Continuity of the deflections and the rotation angles at the end of the overlap were imposed as boundary conditions, and the bending stiffness of the overlap was calculated by assuming that the upper and lower adherends were lumped together. By applying the approximations

$$\sinh u_1 l \approx \cosh u_2 l \approx \tfrac{1}{2}e^{u_1 l},$$

to the isotropic balanced single-lap joint, the edge moment, M_o can be determined as

$$M_o = k\frac{Tt}{2} = \frac{kpt^2}{2}, \tag{3}$$

and

$$k = \frac{\cosh(u_2 c)}{\cosh(u_2 c)+2\sqrt{2}\sinh(u_2 c)} = \frac{1}{1+2\sqrt{2}\tanh(u_2 c)} = \frac{1}{1+2\sqrt{2}\tanh\left(\dfrac{\xi c}{2\sqrt{2}}\right)}, \tag{4}$$

where

$$u_1 = \xi = \sqrt{\frac{12(1-\nu^2)T}{Et^3}} \quad \text{and} \quad u_2 = \frac{\xi}{2\sqrt{2}}.$$

Thus, the edge moment, M_o (or the normalized edge moment, k) depends only on E, c, t and T.

Goland and Reissner then separated the joints into two cases: (a) relatively inflexible adhesive ($10\eta/t \leqslant E_c/E$); (b) relatively flexible adhesive ($E_c/E \leqslant \eta/10t$). A stress analysis of the joint with an inflexible adhesive was addressed in part II, in which the overall overlap was treated as a single deformed body with the same material properties as the adherend. An approximate solution was obtained by solving the elastic boundary-value problem with given M_o and T at the end of the overlap, and neglecting V_o. The stress distributions for this joint with the 90° corner (i.e. no spew fillet) depend upon parameters M_o (or k), T, E and t. Part III addresses the stress analysis of the joint with a flexible adhesive. Due to the nature of this joint, the assumption is made that the deformations of adherend arise only from the longitudinal stress, σ_x, since the transverse normal strain and shear strain in the adherends are relatively small compared to those in the adhesive. A cylindrically bent-plate formulation was developed with values of M_o, T and V_o from part I. However, large deflections of the overlap were ignored in part III. The adhesive shear and transverse normal stresses (τ_o and σ_o) were assumed constant through the thickness of the relatively thin adhesive layer. The closed-form solutions are given as adhesive shear stress (τ_o):

$$\frac{\tau_o}{p} = -\frac{1}{8}\frac{t}{c}\left[\frac{\beta c}{t}(1+3k)\frac{\cosh\left(\dfrac{\beta c}{t}\dfrac{x}{c}\right)}{\sinh\dfrac{\beta c}{t}}+3(1-k)\right], \tag{5}$$

where

$$\beta^2 = \frac{8G_c t}{E\eta} = \frac{4E_c t}{E\eta(1+\nu_c)};$$

adhesive normal stress (σ_o):

$$\frac{\sigma_o}{p} = \frac{t^2}{c^2}\frac{1}{\Delta}\left[\left(R_2\lambda\frac{^2k}{2}+\lambda k'\cosh\lambda\cos\lambda\right)\cosh\left(\lambda\frac{x}{c}\right)\cos\left(\lambda\frac{x}{c}\right)\right.$$
$$\left.+\left(R_1\lambda\frac{^2k}{2}+\lambda k'\sinh\lambda\sin\lambda\right)\sinh\left(\lambda\frac{x}{c}\right)\sin\left(\lambda\frac{x}{c}\right)\right], \tag{6}$$

where

$$\gamma^4 = 6\frac{E_c}{E}\frac{t}{\eta}$$

$$\lambda = \gamma\frac{c}{t}$$

$$R_1 = \cosh\lambda\sin\lambda + \sinh\lambda\cos\lambda$$

$$R_2 = \sinh\lambda\cos\lambda - \cosh\lambda\sin\lambda$$

$$\Delta = \tfrac{1}{2}(\sinh 2\lambda + \sin 2\lambda)$$

and

$$k = \frac{2M_o}{pt^2} \quad \text{and} \quad k' = \frac{cV_o}{pt^2}.$$

It is important to note that the expression for σ_o [eqn (6)] is that developed by Goland and Reissner. The expression is correct even though Goland and Reissner were inconsistent with the sign of V_o in the boundary conditions of their derivation [see eqns (38) and (48) of the Goland and Reissner paper]. The effect of the inconsistency on σ_o was removed by a second inconsistency in the development of their analysis from eqns (48) to (53). Sneddon (1961) pointed out the inconsistency in Goland and Reissner's formulation of the boundary conditions and removed it [but did not correct eqn (48) in the Goland and Reissner paper]. Sneddon also removed the second inconsistency in the derivation but used the original eqn (48), and obtained an expression similar to eqn (6) but with negative signs for the k' terms (the terms involving the edge shear V_o). Subsequently many researchers have used the Sneddon expression. Should any further evidence be needed that eqn (6) is correct, in addition to the fundamental mechanics, appeal might also be made to the fact that eqn (6) provides a more reasonable model for the cases with a large edge shear, and that it agrees with a two-dimensional finite element analysis more closely than the Sneddon correction.

Hart-Smith (1973)

Hart-Smith presented a detailed analysis which, essentially, combines Goland and Reissner's parts I and III, and takes into account the individual deformations of the upper and lower adherends in the overlap, which is, of course, more realistic than the adoption of the lumped overlap. The Hart-Smith analysis involves the determination of the edge moment, M_o, and adhesive shear and transverse normal stresses (τ_o and σ_o), simultaneously. The M_o obtained from this approach is a function of E, c, t, l, T, E_c and η (recall that E_c and η are not included in the Goland and Reissner's M_o formulation). By neglecting small terms and applying the approximation of $\sinh u_1 l \approx \cosh u_1 l \approx (e^{u_1 l})/2$, the solution for M_o becomes dependent only on E, c, t, η and T (or η and ξc) as:

$$M_o \cong T\left(\frac{t+\eta}{2}\right)\frac{1}{1+\xi c+\dfrac{\xi^2 c^2}{6}} \quad \text{or} \quad k \cong \left(1+\frac{\eta}{t}\right)\frac{1}{1+\xi c+\dfrac{\xi^2 c^2}{6}}. \tag{7}$$

This analysis accounts for the effect of the large deflection in the outer adherend, but disregards the large deflection effect in the overlap.

Oplinger (1991)

Oplinger proposed an even more detailed analysis than Hart-Smith's to account for the large overlap deflection effect. Based on Oplinger's formulation (Appendix B and Oplinger

1991), the normalized edge moment is

$$k = \frac{R_3\left(1+\frac{\eta}{t}+R^2C_2\right)+8R_4\frac{T_{h21}}{T_{h22}}R\left[C_1\left(1+\frac{\eta}{t}\right)-C_2\right]}{R_3+8R_4\frac{T_{h21}}{T_{h22}}RC_1+\sqrt{8}(1+R^2C_1)\frac{T_{h21}}{T_{h1}}}, \tag{8}$$

where

$$R = \sqrt{24\frac{p\eta(1+v_c)}{tE_c}}$$

$$R_3 = \sqrt{\frac{8v_1}{R}}$$

$$R_4 = \sqrt{\frac{v_2}{8}}$$

$$v_1, v_2 = a \pm b, \quad a = \left[4\left(1+\frac{3\eta}{4t}\right)+\frac{R^2}{4}\right], \quad b = \sqrt{a^2-R^2}$$

$$C_1 = \frac{K_1}{K_2}$$

$$C_2 = \frac{1}{K_2}$$

$$K_1 = \frac{3}{4}\left(\frac{1}{R_4^2-\frac{R^2}{16}}\right), \quad K_2 = 48\left(\frac{R_4^2}{4R_4^2-1}\right)$$

$$T_{h1} = \tanh\left(l\sqrt{\frac{12(1-v^2)T}{Et^3}}\right) = \tanh(\xi l)$$

$$T_{h21} = \tanh\left(\mu_1\frac{c}{t}\right)$$

$$T_{h22} = \tanh\left(\mu_2\frac{c}{t}\right)$$

$$\mu_1 = \frac{R_3}{\sqrt{8}}R\sqrt{\frac{G_c(1-v^2)t}{E\eta}}, \quad \mu_2 = \sqrt{8}R_4\sqrt{\frac{G_c(1-v^2)t}{E\eta}}.$$

General comments on the above three treatments

In part I of the Goland and Reissner analysis, the calculation of the edge moment, M_o, took into account the influence of the large deflection of the overlap (called the geometrically nonlinear effect), while the stress analysis of the overlap, in parts II and III, ignored this effect. Thus, the M_o expression is valid for short and long overlaps, but the stress analysis of the overlap is reliable only for a short overlap, unless the stress transfer from the upper adherend to the lower adherend is insensitive to the geometrically nonlinear effect. Since the assumption of the lumped overlap in Goland and Reissner's model may not be realistic, Hart-Smith removed this limitation by considering the individual deformations of the upper and lower adherends for the overlap. The Hart-Smith model is, however, still limited to the short overlap with a relatively thin flexible adhesive, as a result of neglecting the large deflection effect in the overlap. The more complete and complex model postulated by Oplinger aimed to improve the Hart-Smith model with the inclusion of the large deflection

effect in the overlap. However, Oplinger's model is still limited to an overlap with a relatively thin and flexible adhesive.

EVALUATION OF THEORETICAL TREATMENTS

Modified Goland and Reissner's solution

The original equation for the normalized edge moment k from Goland and Reissner's analysis [eqn (4)] for the isotropic balanced single-lap joint depends only on ξc, due to the elimination of the parameter l through the approximations of $\sinh(u_1 l) \approx \cosh(u_1 l) \approx (e^{u_1 l})/2$. A modification to part I of Goland and Reissner's analysis, the determination of k, is proposed here to include the presence of the adhesive layer and the length of outer adherend (i.e. parameters E_c, η and l). The detailed derivations are presented in Appendix A in which eqn (A.8) is the general solution, which can be recovered as eqn (4), the original Goland and Reissner solution, if $\eta = 0$ and the approximations for $u_1 l$ is included. To investigate the effect of the outer adherend length on k for the balanced single-lap with the zero thickness of adhesive (i.e. $\eta = 0$ and $u_1/u_2 = 2\sqrt{2}$), eqn (A.8) becomes:

$$k = \frac{1}{1 + 2\sqrt{2}\tanh\left(\frac{\xi c}{2\sqrt{2}}\right)\coth(\xi l)}. \tag{9}$$

Equation (9) is plotted in Fig. 3 for $l/c = 0.1 \sim 100$, in which it is apparent that there is not a single k–ξc curve, but a family of curves gradually converging as $l/c > 100$, and $k = 1$ as ξc approaches 0. The k–ξc curves for $l/c < 1$ are significantly different to those when $l/c = 5 \sim 100$. Furthermore, all k–ξc curves converge asymptotically to $k = 0.26$ for large values of ξc.

Definition of short and long joints

Since Goland and Reissner's analysis neglected large overlap deflection effect in part III, it is interesting to determine how such nonlinear behavior affects the edge moment, and under what conditions the nonlinear effects are negligible. If the overlap is relatively long compared to the thickness of the adherend, the large deflection of the overlap should be

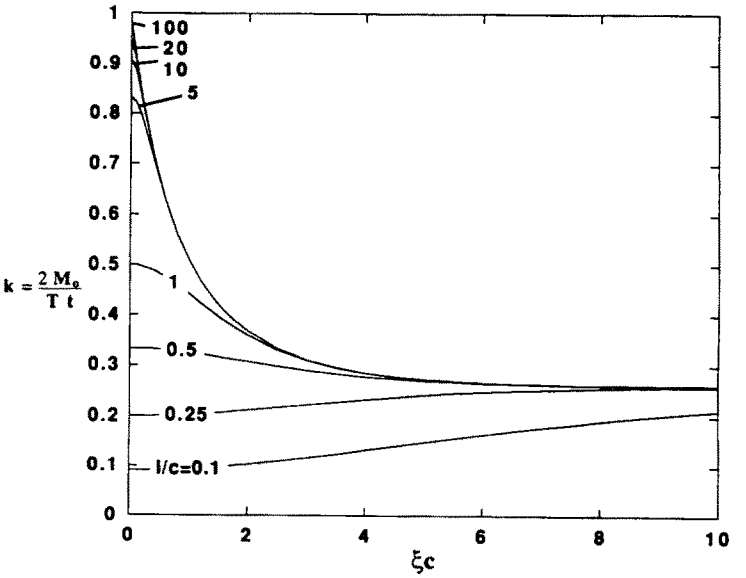

Fig. 3. The normalized edge moment k vs ξc for the original Goland and Reissner analysis with variation of l/c.

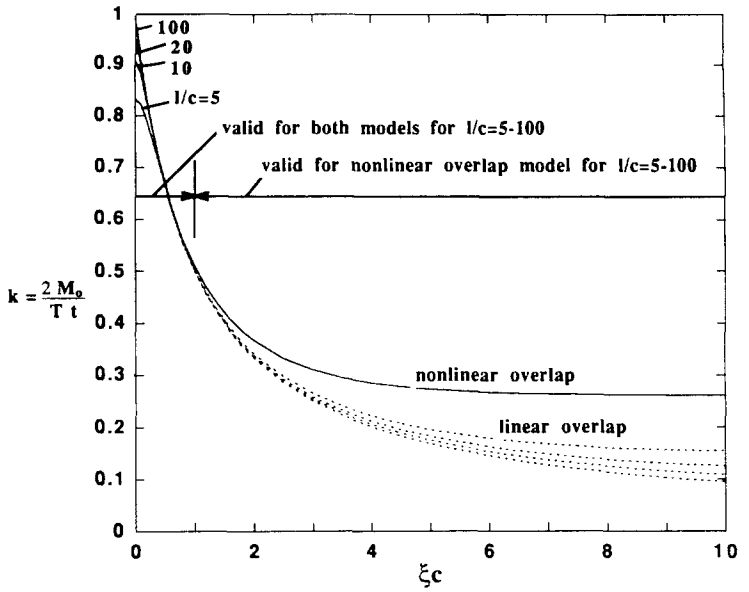

Fig. 4. k–ξc curve comparison of overlap geometrically linear and nonlinear models based on Goland and Reissner's theory.

included in the analysis. If the overlap is not long enough to manifest this large deflection effect before it fails, the effect can be ignored in the analysis. The former is defined as the long joint and the latter as the short joint. It is now proposed to address the issue of distinguishing these cases.

The k formulation, based on part I of Goland and Reissner, is developed in Tsai and Morton (1992a) neglecting the large overlap deflection effect. The new equation for k is compared to the original eqn (4) in the plot of k vs ξc in Fig. 4. Initially the k–ξc curves are superimposed for the linear and nonlinear overlap deflections in the range $l/c = 5 \sim 100$, while they diverge beyond $\xi c = 1$. Thus the linear formulation of the overlap is still valid for $\xi c \leqslant 1$. In other words, provided that $\xi c \leqslant 1$, there are no significant effects of the overlap geometric nonlinearity on the joint edge moment. Based on this observation, short overlaps can be defined simply as $\xi c \leqslant 1$ (or about $c/t \leqslant 0.31\sqrt{E/p}$, taking $\nu = 0.34$), and the long overlap when $\xi c \geqslant 1$. When p (applied average stress) reaches σ_u (the strength of the adherend), which is approximately the maximum applied stress or, in most cases, less than that, due to the presence of the bending moment, the corresponding maximum value of ξc can be determined. Thus the geometric and material parameters of the short joint can be defined as:

$$\frac{c}{t} \leqslant 0.31\sqrt{\frac{E}{\sigma_u}}. \tag{10}$$

From eqn (10), balanced single-lap joints for a range of materials can be classified as short and long joints in terms of the value of c/t, as depicted in Fig. 5.

Hart-Smith's complete solution

Hart-Smith identified a limitation of part I of Goland and Reissner's treatment, the assumption of the lumped overlap, and suggested an improved solution for k by considering the presence of the adhesive layer. His solution is, however, limited to the geometrically linear deformation of the overlap. Instead of the simplified formulation of k [eqn (7)], which is only a function of η and ξc, the complete procedure and formulations are reviewed and described in Tsai and Morton (1992a) in order to incorporate parameters l and E_c into the calculation of k. The simultaneous algebraic equations were employed to calculate k,

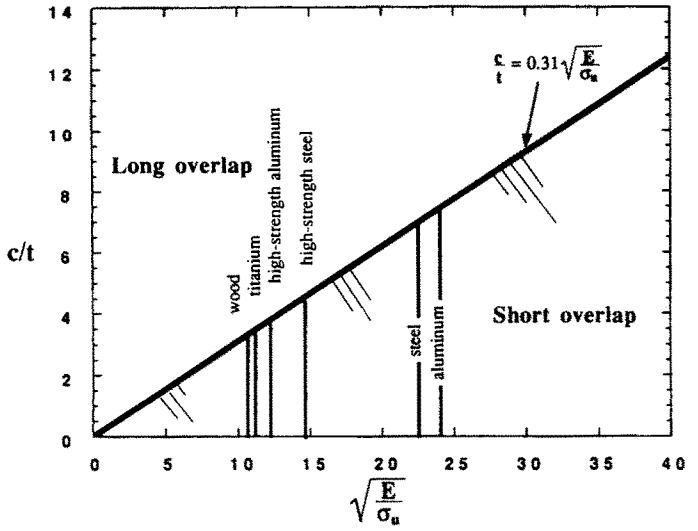

Fig. 5. Definition of long and short overlap joints.

compared to the simple solution, and illustrated graphically in Fig. 6 for the case of $\eta/t = 0.078$ with several values of l/c and E_c/E. It is evident that, in Hart-Smith's analysis, changes in l/c do affect the k value for small values of ξc (note that k approaches 1.078 rather than 1, due to the thickness effect of the adhesive layer). It is also apparent in the complete solution that the parameter E_c/E can influence substantially the k–ξc behavior within the region of large values of ξc, not apparent in the simplified solution.

NUMERICAL ANALYSES

The problem of the single-lap joint has geometrically nonlinear features resulting from the off-axis applied force (eccentricity of loading path) which cause large rotations of the

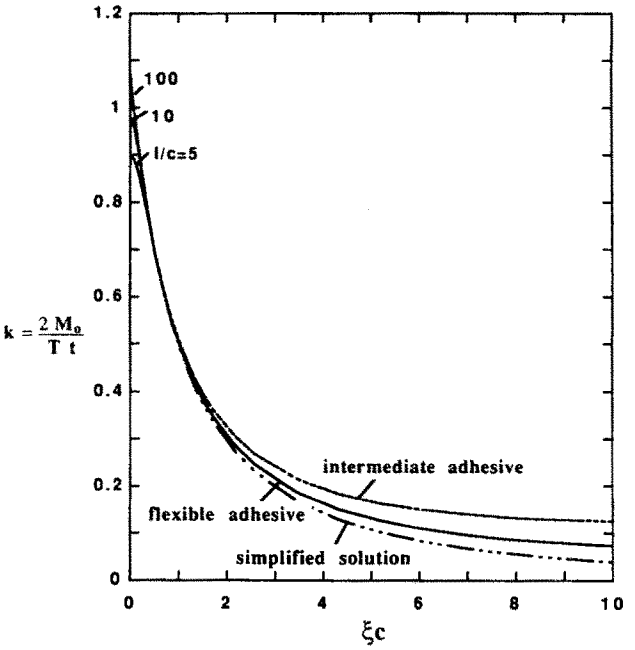

Fig. 6. k–ξc curves obtained from Hart-Smith's model with complete solutions (with E_c/E effect) and simplified solution, eqn (7) (without E_c/E effect) for $\eta/t = 0.078$ and $l/c = 5 \sim 100$.

overlap. The off-axis loading is mainly a result of the discontinuity in the neutral axes between the outer adherend and the overlap. The transverse deflection due to applied loads is coupled with the loading, so that this highly geometrically nonlinear problem cannot be solved through the geometrically linear approach. In this study, a geometrically nonlinear, two-dimensional plane-strain finite element analysis with material linearity is used to determine the edge moment, analyse the stress state of the adhesive layer and assess the closed-form solutions.

A two-dimensional plane-strain finite element analysis with a geometric nonlinearity, from Zienkiewicz (1977), with a nonlinear strain–displacement relationship (Green's strain tensor), was performed. This strain–displacement relationship, in the Cartesian system of x and y coordinates with corresponding displacements u and v, is:

$$\varepsilon_x = \frac{\partial u}{\partial x} + \frac{1}{2}\left[\left(\frac{\partial u}{\partial x}\right)^2 + \left(\frac{\partial v}{\partial x}\right)^2\right]$$

$$\varepsilon_y = \frac{\partial v}{\partial y} + \frac{1}{2}\left[\left(\frac{\partial u}{\partial y}\right)^2 + \left(\frac{\partial v}{\partial y}\right)^2\right]$$

$$\gamma_{xy} = \frac{\partial u}{\partial y} + \frac{\partial v}{\partial x} + \left[\frac{\partial u}{\partial x}\cdot\frac{\partial u}{\partial y} + \frac{\partial v}{\partial x}\cdot\frac{\partial v}{\partial y}\right]. \tag{11}$$

The numerical calculations in this study were performed using ABAQUS, a commercial finite element code, which employ's Newton's method as the nonlinear equation solver.

The schematic representation of the specimen geometry (Fig. 7), contains the geometric

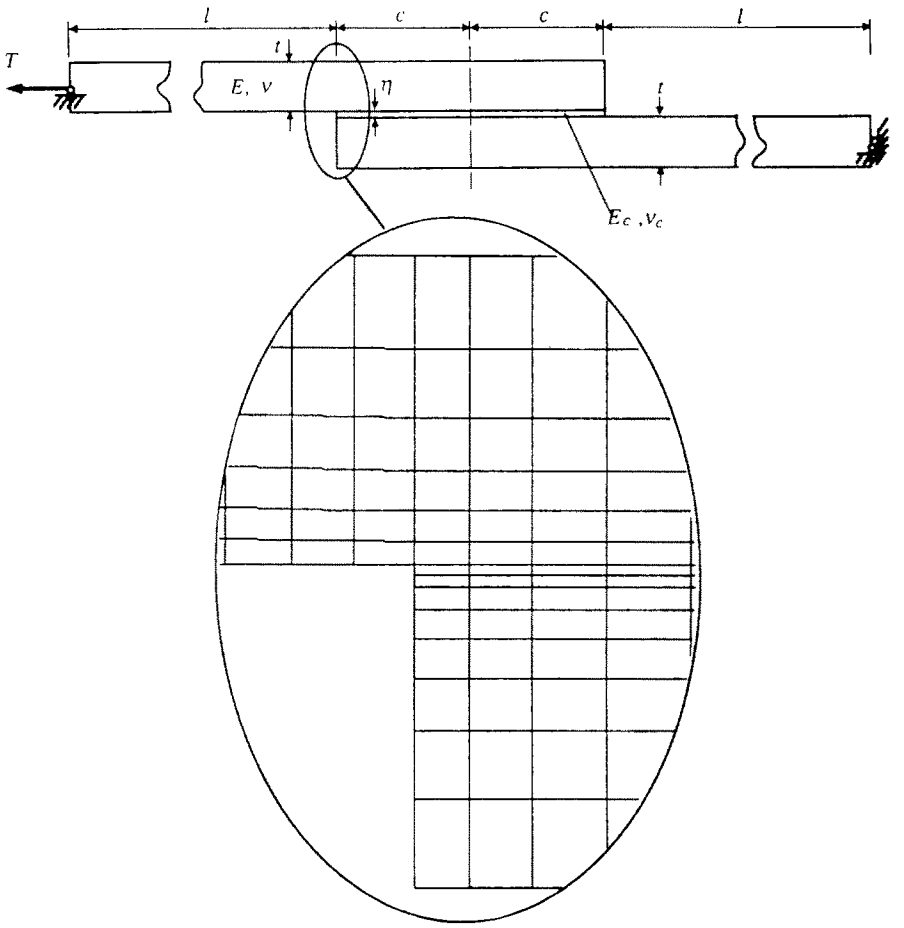

Fig. 7. Specimen geometry and detailed mesh used in the present finite element analysis.

and material parameters, the boundary conditions, as well as the detailed finite element mesh. The boundary conditions applied here consist of a hinge at one side end of the specimen and a roller at the other, located in the neutral axes of the outer adherends, which allow the resultant force to act through the center point of the overlap, and thus generate the antisymmetric loading and geometry conditions. The finite element mesh contains 2 constant-strain elements through the thickness of the adhesive layer and 6 elements through the thickness of the adherend. Since only 2 constant-strain elements were used, the values of the adhesive stresses along the center line of the adhesive layer are close to the average of those over the thickness of the adhesive layer.

Numerical investigations for the stress analyses of a typical short joint, a typical long joint, and joints ranging from the former to the latter, are presented. For all cases, the parameters E, ν, t and ν_c are $E = 70$ GPa, $\nu = 0.34$, $t = 1.6$ mm and $\nu_c = 0.4$, respectively, and $\sigma_u = 500$ MPa. For the short joint analyses, $l/c = 10$, $c/t = 4$, $\eta/t = 0$, 0.078 and 0.158, and $E_c/E = 0.08$, 0.04 and 0.008 (which represent relatively inflexible, intermediate flexibility, and flexible adhesive layers, respectively, for $\eta/t = 0.078$). For the long joint case, the relevant parameters were taken as $l/c = 1.25$ and 5, $c/t = 32$, $\eta/t = 0.078$, and $E_c/E = 0.04$ (intermediate) and 0.008 (flexible). For the joints ranging from the short to long, the values of the parameters were $l/c = 5$, $\eta/t = 0.078$ (with intermediate flexibility adhesive), and $E_c/E = 0.04$, and c/t ranging from 4 to 32.

Typical short joint

The transverse deflections (normalized by the adherend thickness t) for various loads (T) are plotted for $\eta/t = 0$ (no adhesive layer) and compared to the Goland and Reissner (GR) solutions in Fig. 8. In the numerical calculation, it should be noted that the maximum variation of calculated deflections across the thickness of the adherend is less than 1%, for the entire loading history. The results in Fig. 8 indicate that the general trends of the deflection curves for the numerical and analytical solutions are in good agreement with each other, and show almost straight line behavior in the joint overlap (a rigid-body rotation) during the entire loading, even near the maximum load. The large slope (or rotation angle) near the junction of the joint overlap and outer adherend (point A in Fig. 8), leads to the large variation in deflection with a small change of x/l. For example, the deflection at the end of overlap has 10% difference between both solutions close to failure load ($T = 800$ N mm^{-1}).

The numerically determined transverse deflection data can be used to obtain the edge moment (or k) as:

$$M_o = T(\alpha_n l - (\text{deflection})_{x=l}) \quad \text{or} \quad k = \frac{2}{t}(\alpha_n l - (\text{deflection})_{x=l}) \tag{12}$$

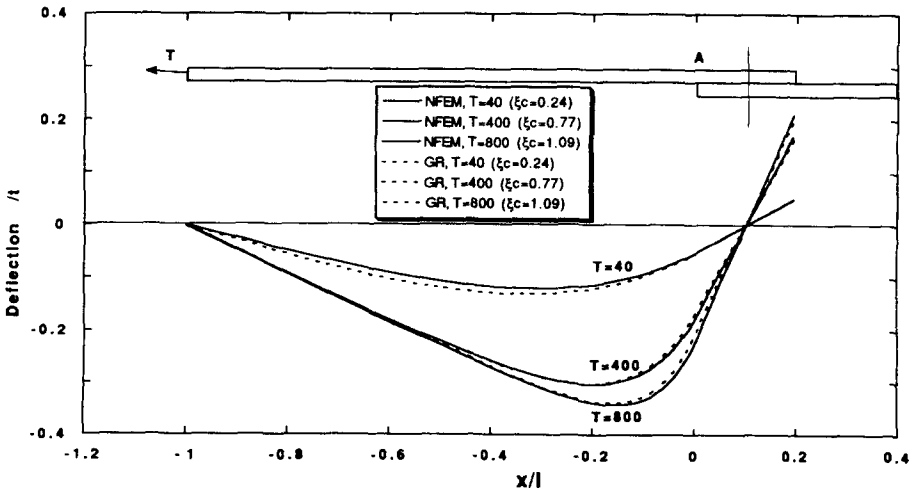

Fig. 8. Comparison of the transverse deflections along the longitudinal direction between nonlinear finite element method (NFEM) and Goland and Reissner (GR) for the short joint with $\eta/t = 0$.

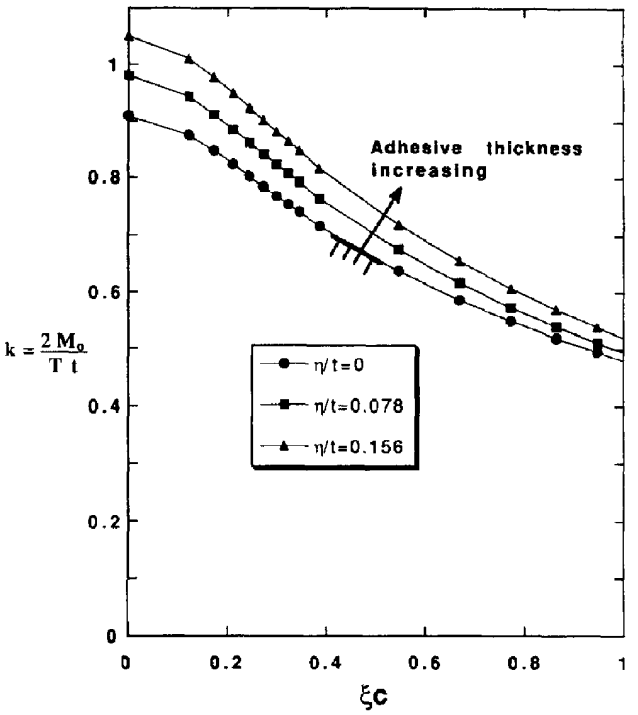

Fig. 9. k–ξc curves obtained from nonlinear finite element method (NFEM) for the short joint with an intermediate flexibility adhesive and $\eta/t = 0 \sim 0.156$.

where

$$\alpha_m = \frac{t+\eta}{2(l+c)}.$$

Equation (12) follows from eqn (A.1) with $x_1 = l$. If eqn (12) were not used in the calculation of the edge moment but the longitudinal normal stress (σ_x) distribution data

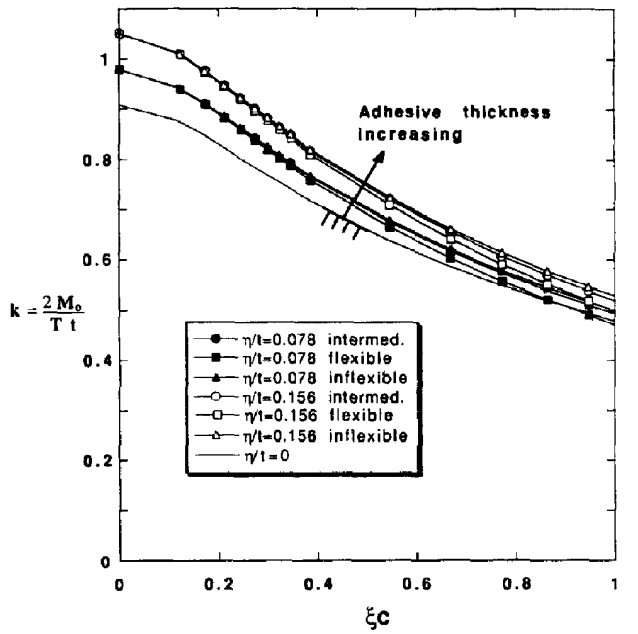

Fig. 10. k–ξc curves obtained from nonlinear finite element method (NFEM) for the short joint with various material properties and thicknesses of the adhesives.

were used, inaccurate results could be obtained since these stress distributions are not perfectly linear, especially close to the interface. The k–ξc curves for the short joint were obtained for a variety of η/t and E_c/E, and presented in Figs 9 and 10, respectively. The calculated stress distributions along the center of the adhesive layer are shown in Fig. 11 for $\eta/t = 0.078$ and $E_c/E = 0.008$ (a relative flexible adhesive layer) for several load cases.

Typical long joint

Transverse defections for the typical long joint are shown in Fig. 12(a) for $l/c = 5$, $c/t = 32$, $\eta/t = 0.078$, and $E_c/E = 0.04$, under various loads. The results of the numerical

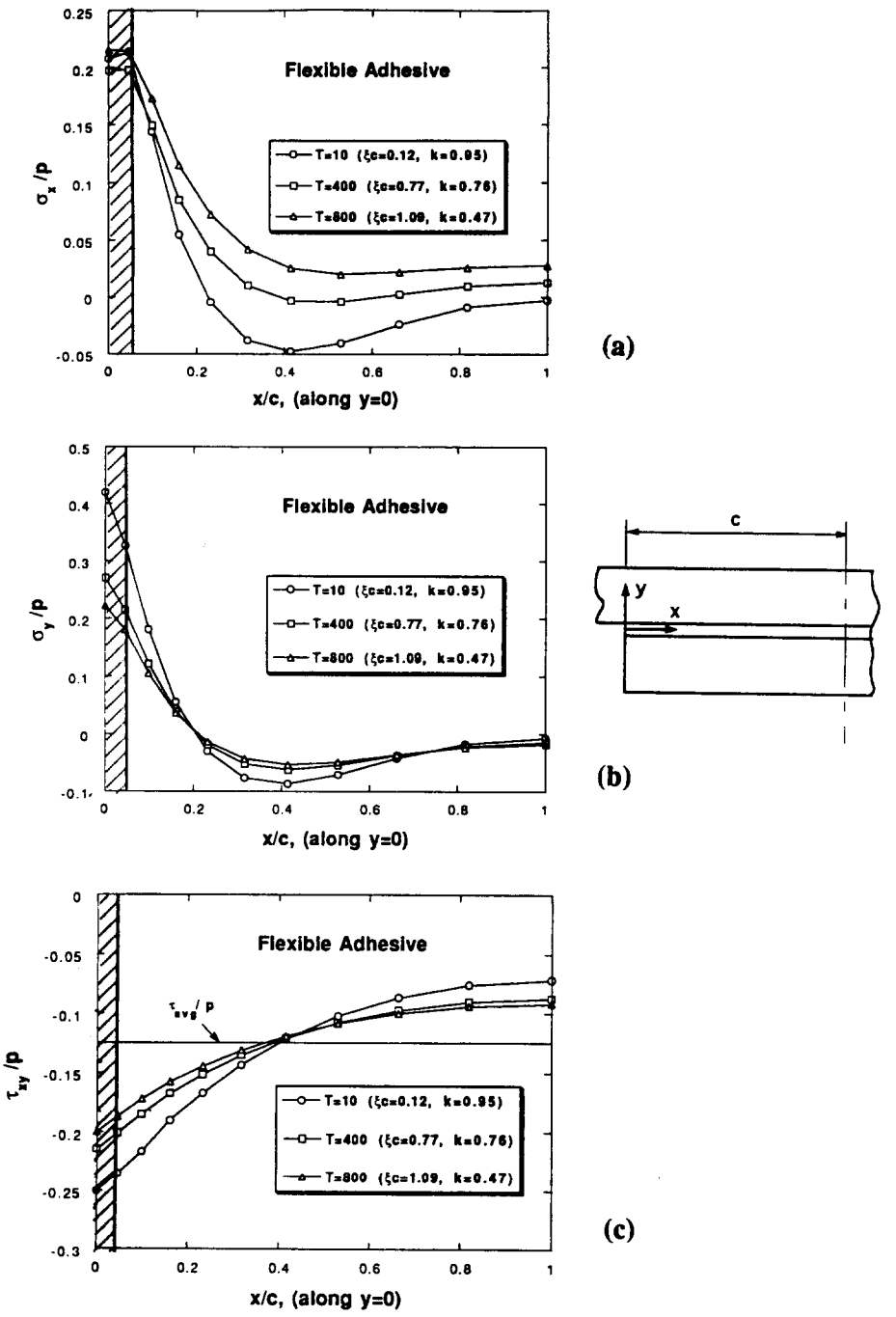

Fig. 11. Adhesive stress distributions, (a) σ_x, (b) σ_y, (c) τ_{xy}, obtained from nonlinear finite element method (NFEM) for the short joint with a flexible adhesive and $\eta/t = 0.078$.

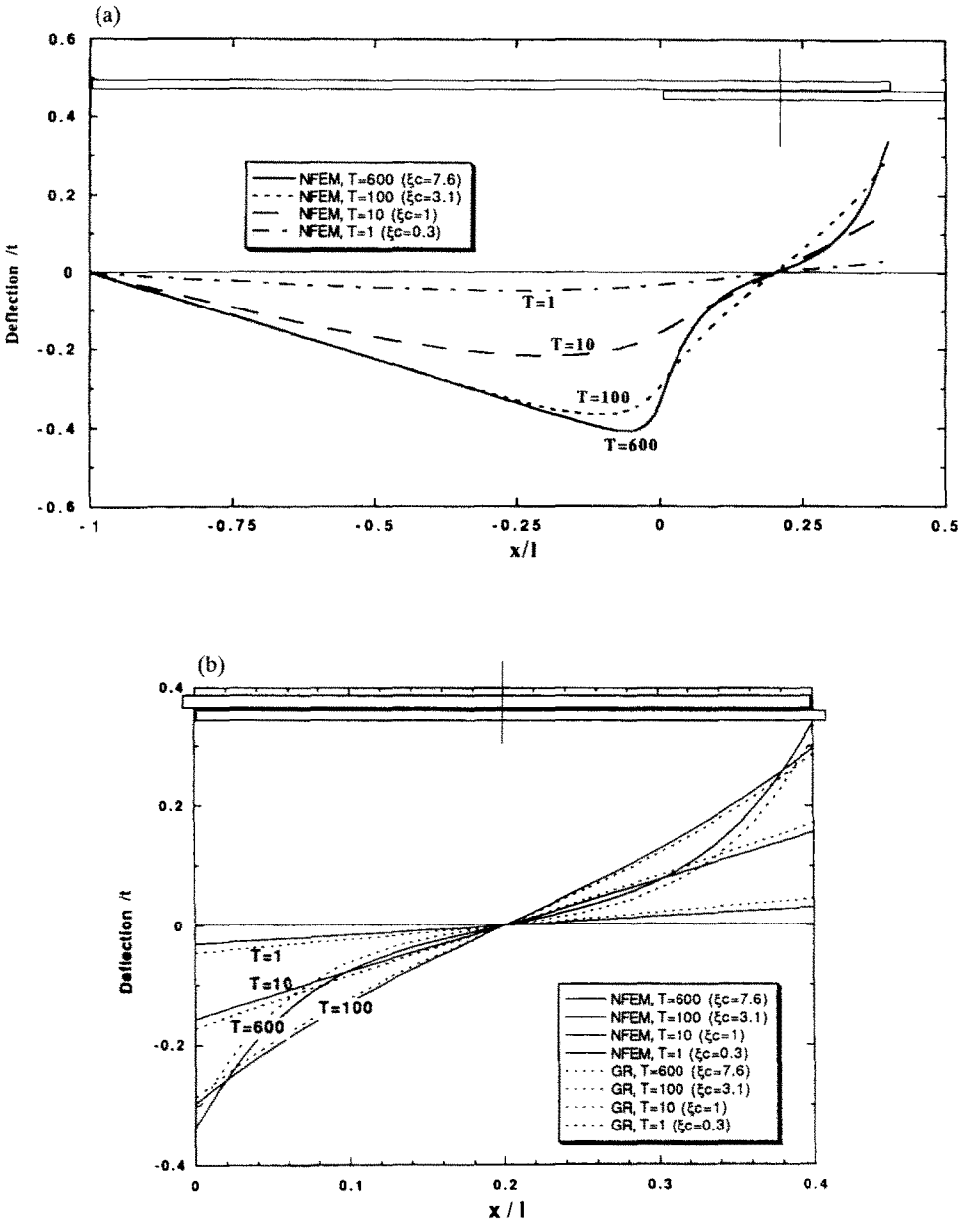

Fig. 12. Transverse deflections (a) obtained from nonlinear finite element method (NFEM), (b) compared to Goland and Reissner (GR) only along the overlap, for the long joint with an intermediate flexibility adhesive and $\eta/t = 0.078$.

analysis indicate that the deformations in the low loading state have features similar to those of the short joint, but with obvious differences, especially near and along the overlap, at high load levels. The detailed comparisons of the deflection of the overlap for the numerical and Goland and Reissner's solutions are presented in Fig. 12(b). Both results show the similar deflected shape, but the differences in the deflections become significant in the edge moment calculations.

The k–ξc curves determined from the nonlinear finite element method (NFEM) and eqn (12) are shown in Fig. 13 for long joints with $c/t = 32$, $\eta/t = 0.078$, $E_c/E = 0.04$, and $l/c = 1.25$ and 5, and in Fig. 14 for $l/c = 5$ and $E_c/E = 0.04$ (intermediate flexibility) and 0.008 (flexible). In Fig. 13 the same effects of the values of l/c on the k–ξc curves as for Goland and Reissner's model in Fig. 3 are observed. The corresponding adhesive stress distributions are shown in Fig. 15 for various applied loads.

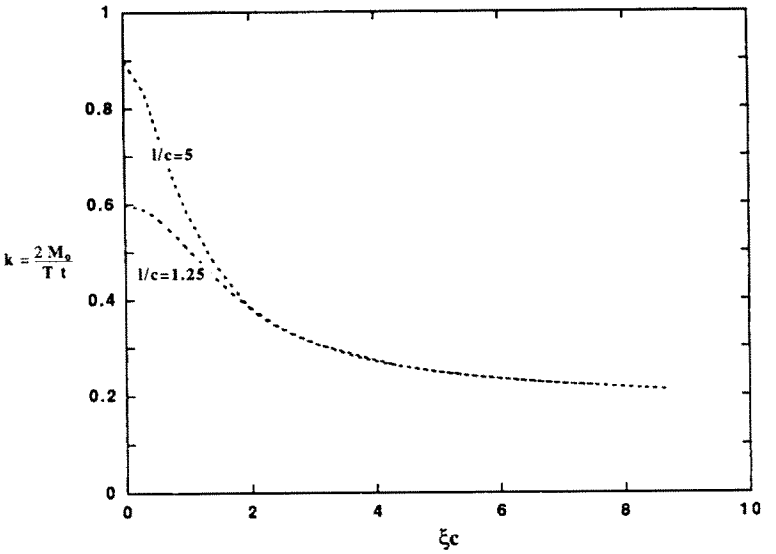

Fig. 13. k–ξc curves determined from nonlinear finite element method (NFEM) for long joints with $l/c = 5$ and 1.25, and an intermediate flexibility adhesive and $\eta/t = 0.078$.

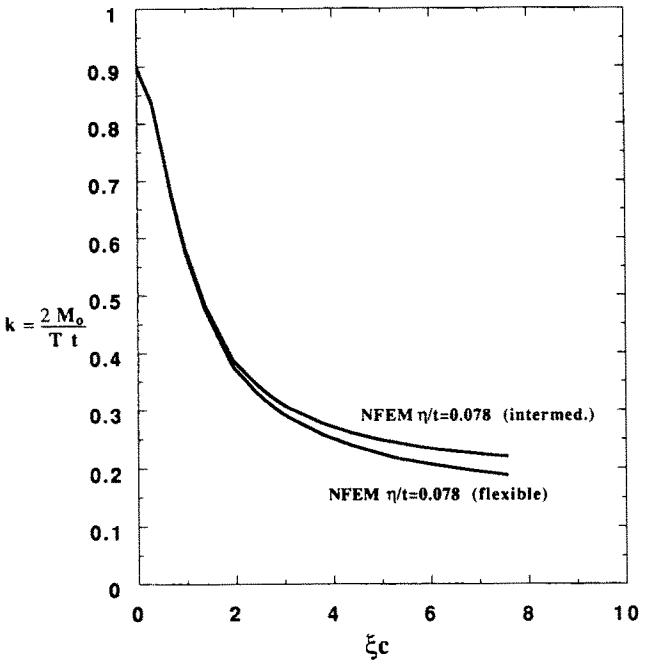

Fig. 14. k–ξc curves determined from nonlinear finite element method (NFEM) for the long joint with an intermediate flexibility and flexible adhesives, and with $\eta/t = 0.078$.

RESULTS AND DISCUSSION

There are two key issues to be addressed: the determination of the edge moments (i.e. k–ξc curves) and the adhesive stress distributions. In order to address the former, the results obtained from the nonlinear finite element analysis are discussed in detail and compared to the closed-form solutions of Goland and Reissner, Hart-Smith and Oplinger. For the latter, the adhesive stress distributions determined from the nonlinear finite element analysis with

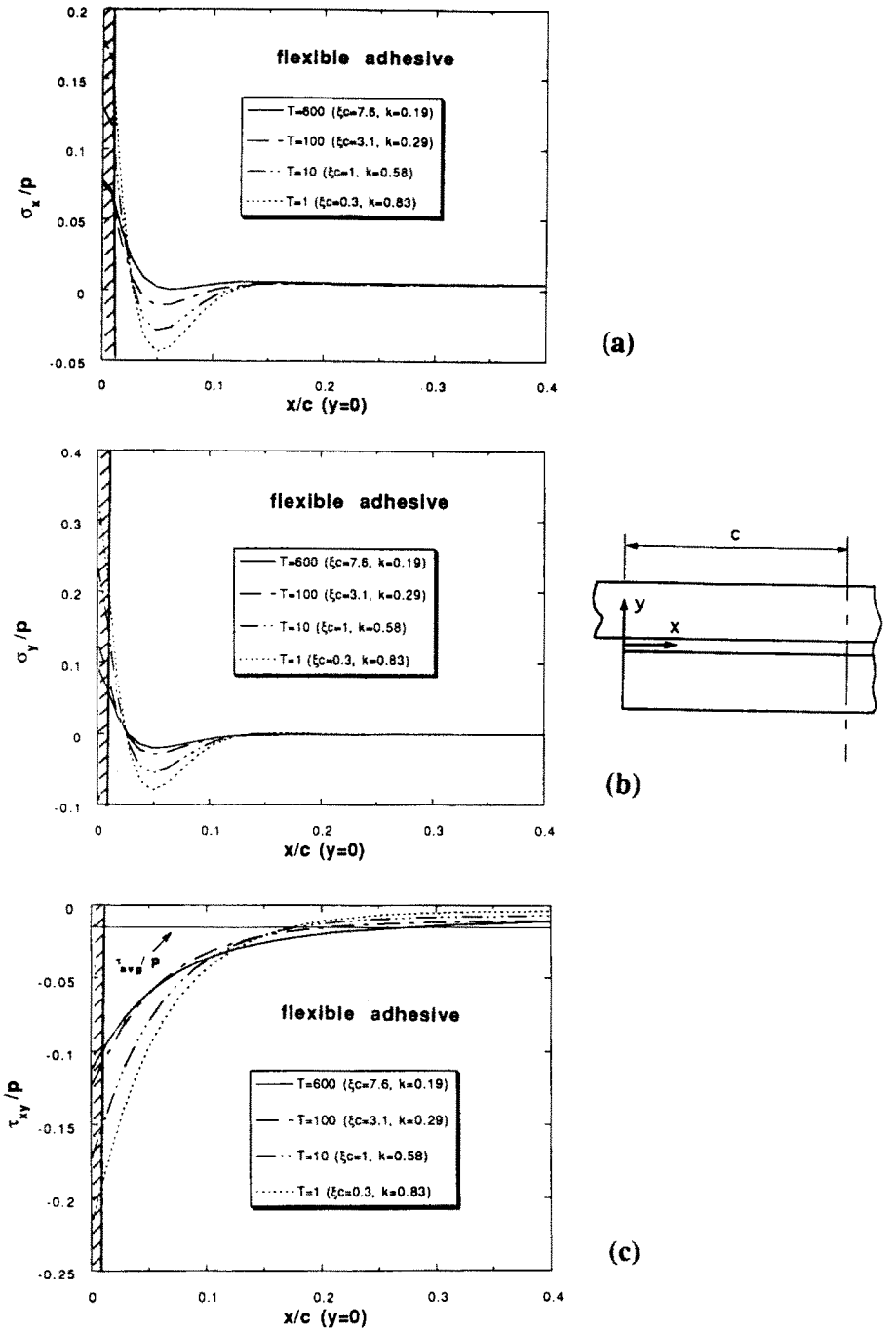

Fig. 15. Adhesive stress distributions, (a) σ_x, (b) σ_y, (c) τ_{xy}, obtained from nonlinear finite element method (NFEM) for the long joint with a flexible adhesive and $\eta/t = 0.078$.

a relatively fine mesh are correlated with the Goland and Reissner solutions for the short and long joints so as to provide a global indication of the load transfer from the one adherend to the other through the adhesive layer.

k–ξc curves

For the short joint, the numerical results shown in Figs 9 and 10 represent the variations of k–ξc (or M_o–ξc) curves with changes in η/t and E_c/E, individually. It is clear, from Fig. 9, that the k–ξc curves shift with the variation of η/t from 0 to 0.156 (with an approximate scale factor of $1+\eta/t$). Also, it is remarked that the convex nature of these curves, for low values of ξc ($0 \leqslant \xi c \leqslant 0.15$), is attributed to the l/c effect (in this case, $l/c = 10$), and these

curves are valid over the entire loading history until adherend failure, for this specific geometry and adherend material. The results shown in Fig. 10 indicate that the k–ξc curves for this short joint are not sensitive to the variation of E_c/E ranging from flexible to inflexible adhesives, especially for ξc values less than 0.8. Even at the maximum value of ξc ($\xi c = 1$), maximum variation of k due to E_c/E effect is still less than 6%.

The comparisons of the numerical short joint and theoretical results in the form of k–ξc curves are provided in Fig. 16. Figure 16(a) contains a detailed comparison with the

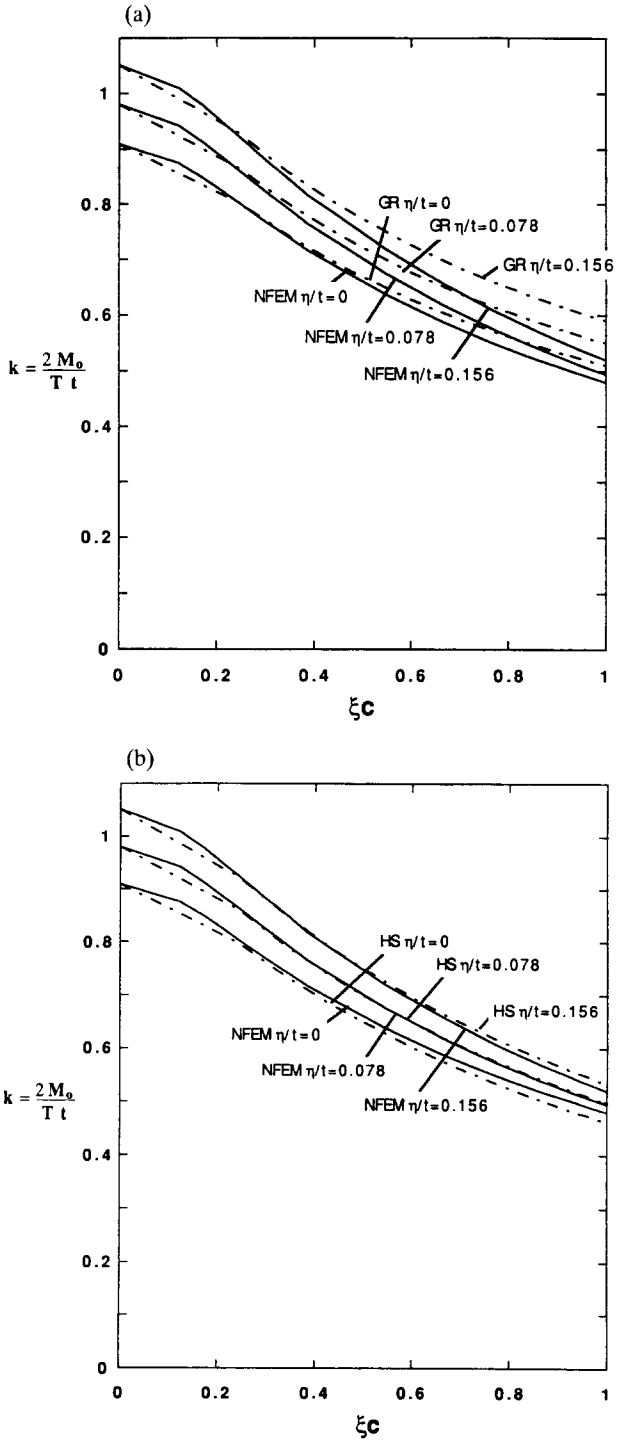

Fig. 16. Comparisons of k–ξc curves obtained from nonlinear finite element method (NFEM) and (a) modified Goland and Reissner (GR), (b) Hart-Smith (HS), (c) Oplinger (OP) models for the short joint with an intermediate flexibility adhesive and $\eta/t = 0 \sim 0.156$.

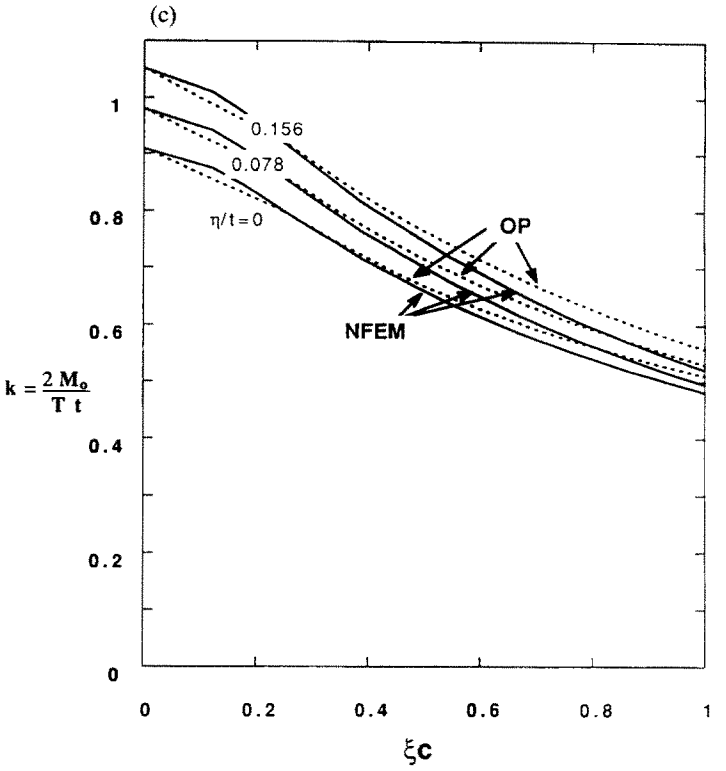

Fig. 16—*continued.*

modified Goland and Reissner solution which incorporates the l/c and the adhesive thickness effects. It is shown that for $\xi c \leqslant 0.5$ the k–ξc curves for a variety of η/t are in reasonable agreement, while for $\xi c \geqslant 0.5$ the differences between both results are somewhat more than 5% (for $\xi c = 1$, 14% difference at $\eta/t = 0.157$, and 8% difference at $\eta/t = 0$). Moreover, Fig. 16(b) contains a comparison of the numerical results and the Hart-Smith complete solution which includes the l/c effect. It is clear that the k–ξc curves obtained by these two approaches are very similar for various η/t (i.e. maximum difference of k values for these two methods are less than 4%). Thus, the Hart-Smith model does represent an improvement on the Goland and Reissner solution for the short joint by the inclusion of the individual deformations of the upper and lower adherends in the overlap in the analysis. Finally, comparisons between the numerical and Oplinger analyses are shown in Fig. 16(c) in which it is apparent that, for the short joint, Oplinger's k values are also sensitive to the variation of η/t as are the numerical results, but the agreement of the Oplinger model with the numerical results is not as good as that for the Hart-Smith model.

The nonlinear finite element results for the long joint are shown in Fig. 17 and compared to various theoretical values. The results in Fig. 17(a) indicate that the numerical solution for the joint with a moderately thin adhesive layer ($\eta/t = 0.078$) is insensitive to E_c/E for $\xi c < 2$, but shows considerable sensitivity to E_c/E as $\xi c \geqslant 2$, especially for large values of ξc (for example, k is about 15% different for $\xi c = 7$). When compared to the Goland and Reissner solution, the correlation between the numerical and original Goland and Reissner solutions ($\eta/t = 0$) is poor at the beginning and near the end of loading. However, agreement is significantly improved in the modified Goland and Reissner solution ($\eta/t = 0.078$) for $\xi c < 2$. Furthermore, the modified Goland and Reissner analysis appears insensitive to E_c/E, and more conservative, in predicting the edge moment. Another comparison, shown in Fig. 17(b) for the numerical and Hart-Smith solutions, indicates that unlike Goland and Reissner's solution, the Hart-Smith model does show a sensitivity to E_c/E similar to the numerical analysis, although there exists a considerable difference in the predicted value of k. This large difference is thought to be caused by neglecting the large overlap deflection

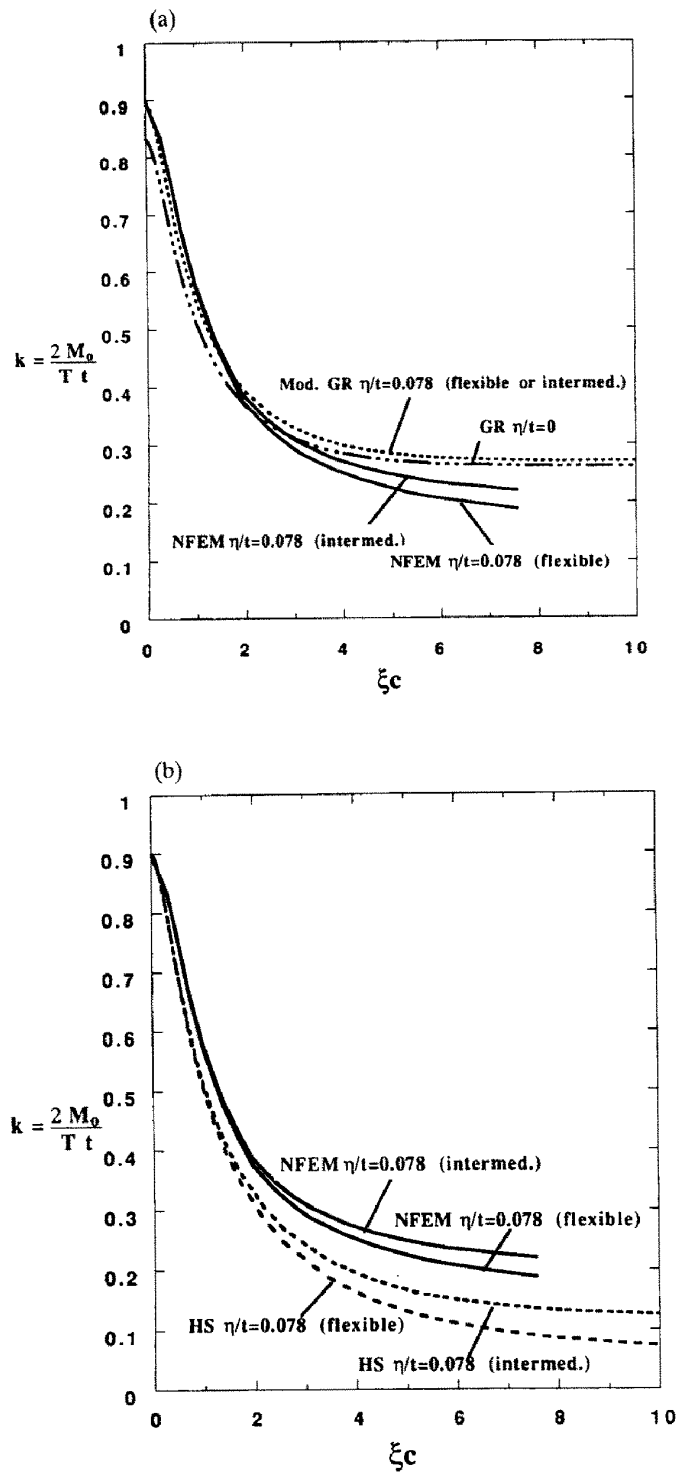

Fig. 17. Comparisons of k–ξc curves obtained from nonlinear finite element method (NFEM) and (a) modified Goland and Reissner (GR), (b) Hart-Smith (HS), (c) Oplinger (OP) models for the long joint with an intermediate flexibility adhesive and flexible adhesives, and $\eta/t = 0.078$.

effects in Hart-Smith's analysis, which is a significant factor in long joints. Finally, the numerical results compared to Oplinger's results are illustrated in Fig. 17(c). It is clear that Oplinger's prediction shows the same E_c/E sensitivity and general trends as the numerical prediction, and agrees with the numerical results more closely than the modified Goland and Reissner and Hart-Smith predictions.

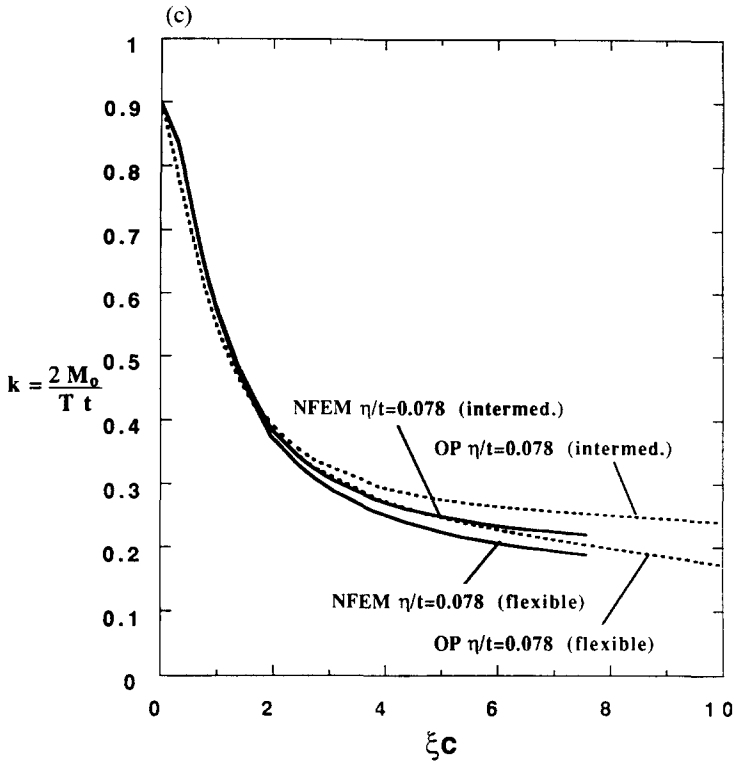

Fig. 17—*continued.*

The k–ξc curves for short and long joints, determined from the numerical analysis, are not coincident, while theoretical models give a single curve for different lengths of the overlap but different curves for the various models. It is interesting to understand how the k–ξc curves evolve from the short joint to long joint. The k–ξc curves calculated using finite element analyses are shown in Fig. 18 for several overlap lengths, and compared to the theoretical models. Note that all the joints were taken to be loaded until adherend failure. It is clear that the k–ξc curves branch out from a single point at the start of loading, for all overlap lengths (or c/t), but end at different values of ξc. The short joint k–ξc curves can be described closely using the Hart-Smith model, whereas the Oplinger model can give better predictions of the long joint behavior. It must also be emphasized that, if geometrically linear analyses were carried out in this case, k would be about 0.9, rather than 1, for these specimens. In order to examine the overlap deformation, the deflection shapes were drawn in Fig. 19 for different overlap lengths which are subjected to the same, near adherend failure load. The results indicate that the overlap deflections remain linear for $c/t = 4$, slightly nonlinear for $c/t = 8$, and extremely nonlinear for $c/t = 32$, before adherend failure. Thus, for the long overlap joint, the large deflection effect is an important factor in determining the edge moment and cannot be ignored, while for the short overlap joint this effect can be neglected.

Adhesive stress distributions

The resulting normalized stress distributions in the adhesive for the short joint with a flexible adhesive under the various loads, shown in Fig. 11, consist of individual stress component (σ_x, σ_y and τ_{xy}) distributions along the center of the adhesive layer for a half of the overlap. The maximum load (stress) applied is the adherend failure load (stress), $T = 800$ N mm^{-1} ($p = 500$ MPa). From these stress distributions, it is observed that there exists a region of stress uncertainty, noted as the shaded area, near the free end, due to violation of stress-free conditions (i.e. $\sigma_x = 0$ and $\tau_{xy} = 0$). Despite the region of stress uncertainty, the location of maximum stress is found to occur at or near the end of the

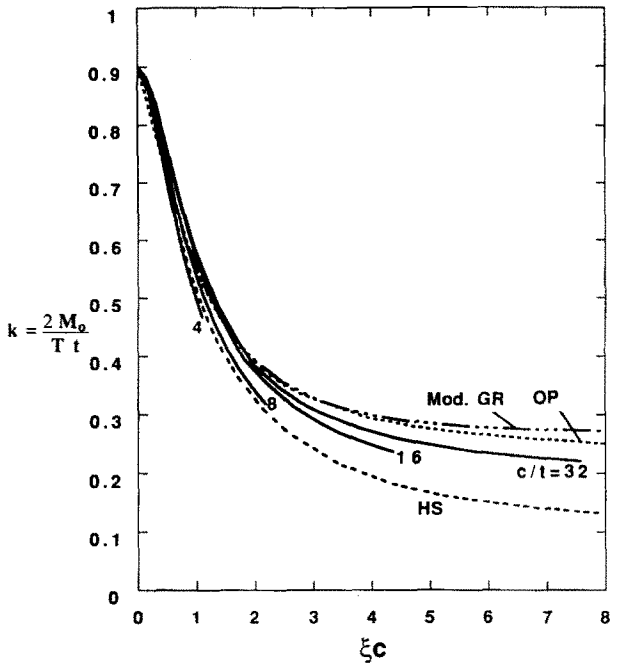

Fig. 18. Comparisons of k–ξc curves determined from nonlinear finite element method (NFEM), modified Goland and Reissner (GR), Hart-Smith (HS), and Oplinger (OP) models for the joints with variation of c/t and values of $l/c = 5$, $\eta/t = 0.078$, and $E_c/E = 0.04$ (intermediate).

overlap, and the normalized stresses (σ_x/p, σ_y/p or τ_{xy}/p) decrease with increasing applied loads. The decreasing normalized stress is caused primarily by the reducing edge moment which results from the large deflection effect. The magnitudes of σ_x near the end of the overlap are comparable to those of σ_y and τ_{xy}, so that the role of σ_x cannot be neglected, especially for accurately determining the σ_y and τ_{xy} in this region. Unfortunately, most of the available theoretical solutions (except Goland and Reissner's part II) do not account for the contribution of σ_x. That is, these theoretical analyses feature one-dimensional (or

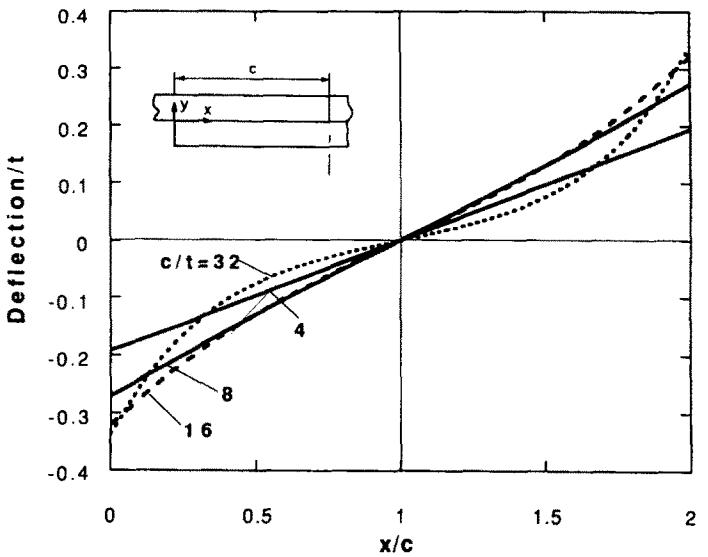

Fig. 19. Transverse deflections along the overlap for the joints with variation of c/t, with the values of $l/c = 5$, $\eta/t = 0.078$, and $E_c/E = 0.04$ (intermediate), and under the same near failure load ($T = 600$ N mm^{-1}).

simplified two-dimensional by assuming $\sigma_x = 0$ in adhesive layer) rather than full two-dimensional analyses. For the σ_y distribution, σ_y acts almost over the entire adhesive layer (about $4t$ from the free end) and large tensile σ_y occurs near (or at) the end of the free end. For the τ_{xy} distributions, it is apparent that the distributions have a tendency to become uniform with increasing the applied loads. The adhesive stress distributions are compared to those from Goland and Reissner's part III, with the corresponding values of k [and k' determined from eqn (2)], in Figs 20(a, b) for σ_y and τ_{xy}, respectively. It is clear that the general trends of the σ_y and τ_{xy} distributions are in reasonable agreement for both results. In terms of maximum stress values, the differences in σ_x or τ_{xy} calculated from these two approaches are within 10%. Also, the stress concentration $(\sigma_y)_{max}/\tau_{avg}$ is about 1.7, while $(\tau_{xy})_{max}/\tau_{avg}$ is about 1.6 for a flexible adhesive under $k = 0.47$ (near the adherend failure load). Note that $\tau_{avg} = T/2c$. It seems likely that the joint adhesive failure is dominated by transverse normal stress, σ_y.

The adhesive stress distributions in Fig. 15 are for the case of the typical long joint under the various loads. These distributions indicate that, like the short joint, there also

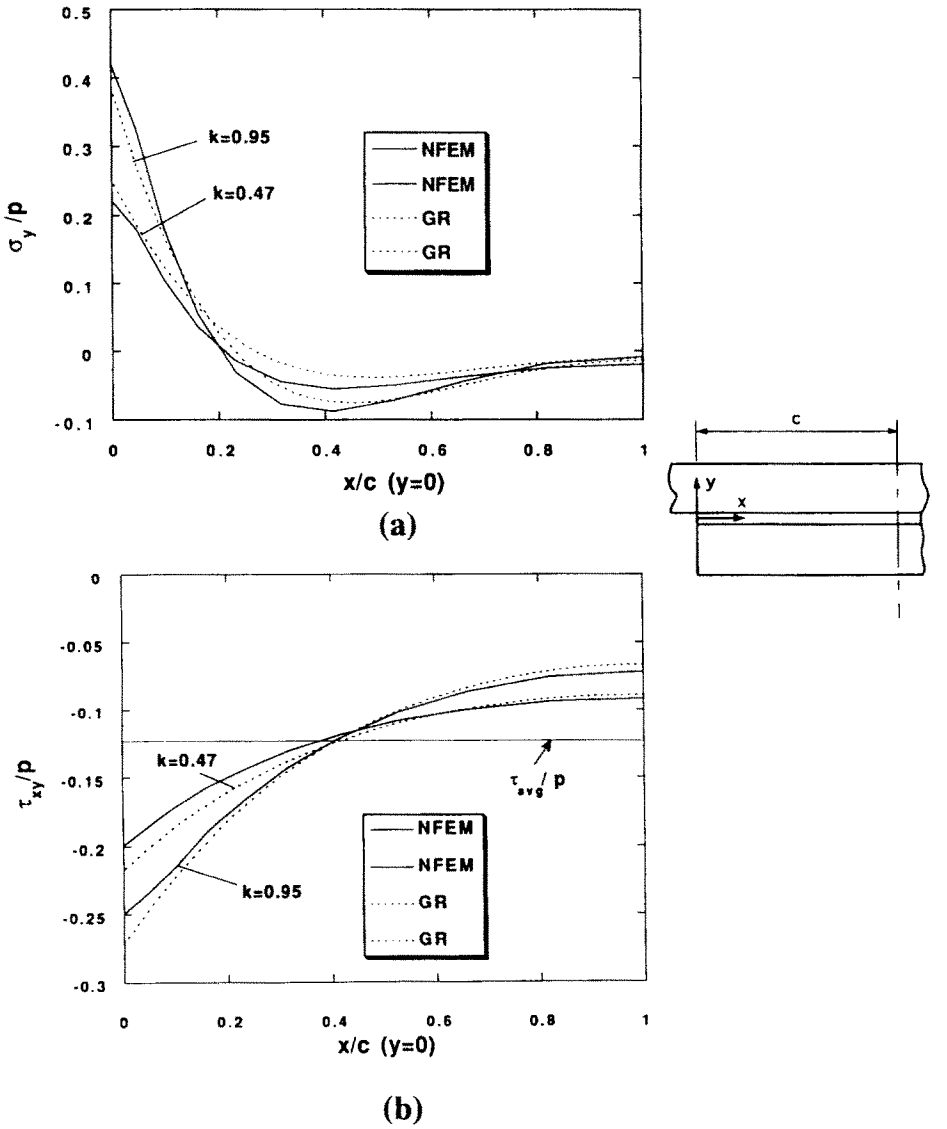

Fig. 20. Comparisons of adhesive stress (a) σ_y, (b) τ_{xy} distributions obtained from nonlinear finite element method (NFEM) and Goland and Reissner (GR) for the short joint with a flexible adhesive and $\eta/t = 0.078$.

exists a region of stress uncertainty and the maximum normalized stresses decrease in value as the applied load increases. It is specially noteworthy that the presence of σ_y is confined to the region of $x/c = 0$ to 0.125 (about a distance of $4t$ from both free ends), and beyond this, the τ_{xy} is almost constant and small. In other words, the zone of significant σ_y is independent of the length of the overlap, and the maximum value of τ_{xy} is not significantly reduced by decreasing τ_{avg}. For example, increasing the length of the overlap from $8t$ to $64t$ (from short to long overlaps) represents a decrease of τ_{avg} from $T/8t$ to $T/64t$ for the same applied load, T, but the maximum σ_y decreases only from 0.42 σ_y/p to 0.24 and the maximum τ_{xy} from 0.25 τ_{xy}/p to 0.17, for the case of $T = 10$ N mm^{-1}. Furthermore, unlike the short joint, the stress concentration $(\sigma_y)_{max}/\tau_{avg}$ is about 5.8 and $(\tau_{xy})_{max}/\tau_{avg}$ is about 7, for $k = 0.187$ (near the adherend failure load). The comparison of the adhesive stress distributions with Goland and Reissner's solution for the low and high applied loads is shown in Fig. 21. It is clear that Goland and Reissner's predictions (part III) are reasonably accurate for the long joint, even though their model (part III) does not include the large deflection effects (or geometric nonlinearity) of the overlap.

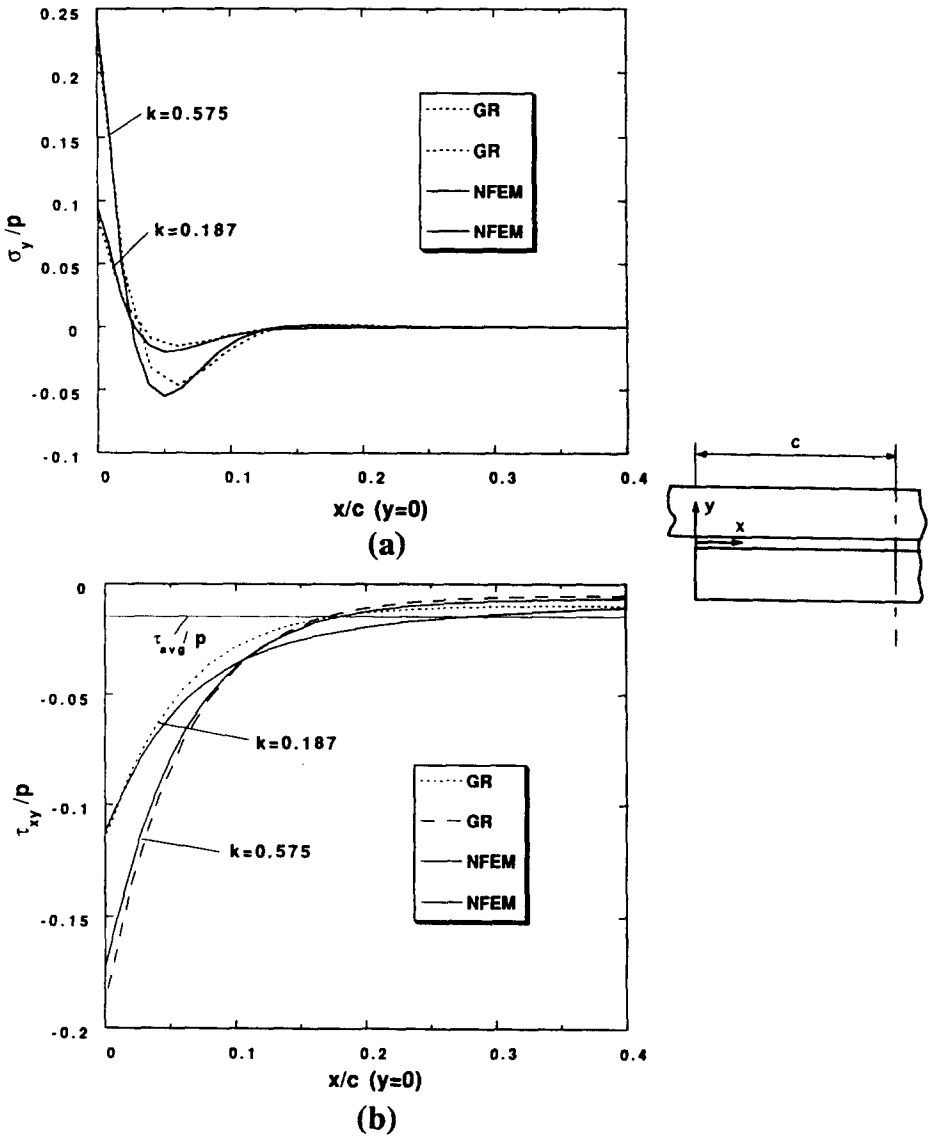

Fig. 21. Comparisons of adhesive stress (a) σ_y, (b) τ_{xy} distributions obtained from nonlinear finite element method (NFEM) and Goland and Reissner (GR) for the long joint with a flexible adhesive and $\eta/t = 0.078$.

The requirement of the stress-free condition at the free ends led Allman (1977), Ojalvo and Eidinoff (1978), Chen and Cheng (1983), and others, to aim at improving Goland and Reissner's part III by means of two-dimensional analyses with the assumption of a constant adhesive shear stress (τ_{xy}) and a linear transverse normal stress (σ_y), or a constant σ_y and a linear τ_{xy}. Likewise, this requirement guided the present finite element analysis with reasonably fine mesh and still produced the region of uncertainty near the free end. It is well known [Williams (1952), Bogy (1971), Bogy and Wang (1971), Hein and Erdogan (1971), Wang and Choi (1982a, b), Tsai and Morton (1992b)] that the stress singularity, which is the unbounded stress state, can be present at the corner (or interface corner) for similar (or dissimilar) materials for linear elastic behavior, and that the strength of the singularity depends on parameters such as the wedge angle and the mismatch of material properties. The bonded joint, of course, contains corners or interface corners which have high stress raisers and which may initiate the failure during loading. A more detailed and localized finite element analysis for this single-lap joint problem has been performed (Tsai and Morton, 1993), which indicates that the strongest stress raiser appears at the interface corners between the loaded adherend and adhesive layer, but not at the other interface corner between the nonloaded adherend and adhesive layer, which results from the very low (or zero) load transfer, although both corners have similar strength of singularity. Therefore, the maximum stresses calculated from the different approaches mentioned above are different and arbitrary, so that the application of maximum stress data to the engineering design of a single-lap joint should be made with caution. Nevertheless, it is true that the validity and practical application of the singular solutions based on linear elastic continuum mechanics are limited to the scale of a local region, and uniform and elastic material behavior, as well as ideal geometry.

CONCLUSIONS

The single-lap joint has been analysed using the geometrically nonlinear finite element method and the results compared to those of the available theoretical solutions. The distinction between the short and long joints has been defined on the basis of the influence of the large overlap deflection on the edge moment. Representative short and long joints were analysed in detail. It is shown that for the short joint, k–ξc curves are sensitive to the adhesive thickness, but not to the adhesive material property, while these curves are sensitive to both factors for the long joint. Moreover, it has been demonstrated that, in contrast to most theoretical models, the k–ξc curves depend on the parameters such as length of the outer adherend (l), adhesive material properties (E_c), thickness of the adhesive (η) and even the length of the overlap ($2c$). Some modifications and corrections to the theoretical solutions have been proposed and suggested for the practical application. The controversy concerning the validity of the theoretical solutions has been resolved and clarified through the definition of the long and short joints and comparisons of numerical and theoretical results. For determination of the edge moment, Hart-Smith's model is more feasible and reasonable for the short single-lap joint with a varied thickness of the adhesive layer than the modified Goland and Reissner and Oplinger models, whereas the Oplinger model gives a more reasonable approximation for the long single-lap joint with variations of thickness and material properties in the adhesive layer. As far as the adhesive stress distributions are concerned, the original Goland and Reissner part III solution, which has been much misquoted and misused, has been demonstrated to be accurate enough to predict the adhesive stress distributions in the global sense for the short and long joint, regardless of its lack of satisfaction of the stress-free conditions in the free end and its neglecting of the large deflection effect in the overlap.

Acknowledgements—The authors appreciate the support of this research by the National Science Foundation Science and Technology Center for High Performance Polymeric Adhesives and Composites at Virginia Tech under contract DMR # 912004. The authors also acknowledge Dr D. W. Oplinger of Federal Aviation Administration Technical Center and Dr L. J. Hart-Smith of McDonnell Douglas Corporation for helpful discussions.

REFERENCES

Adams, R. D. and Peppiatt, N. A. (1974). Stress analysis of adhesively bonded lap joints. *J. Strain Anal.* **9,** 185–196.

Allman, D. J. (1977). A theory for elastic stresses in adhesive bonded lap joints. *Quart. J. Mech. Appl. Math.* **30,** 415–436.

Bogy, D. B. (1971). Two edge-bonded elastic wedges of different material and wedge angles under surface tractions. *J. Appl. Mech.* **38,** 377–386.

Bogy, D. B. and Wang, K. C. (1971). Stress singularities at interface corners in bonded dissimilar isotropic elastic materials. *Int. J. Solids Structures* **7,** 993–1005.

Chen, D. and Cheng, S. (1983). An analysis of adhesive-bonded single-lap joints. *J. Appl. Mech.* **50,** 109–115.

Crocombe, A. D. and Adams, R. D. (1981). Influence of the spew fillet and other parameters on the stress distribution in the single-lap joint. *J. Adhesion* **13,** 141–155.

Goland, M. and Reissner, E. (1944). The stresses in cemented joints. *J. Appl. Mech.* **11,** A17–A27.

Harris, J. A. and Adams, R. D. (1984). Strength prediction of bonded single lap joints by non-linear finite element methods. *Int. J. Adhesion Adhesives* **4,** 65–78.

Hart-Smith, L. J. (1973). Adhesive-bonded single-lap joints. NASA, CR-112236.

Hein, V. L. and Erdogan, F. (1971). Stress singularities in a two-material wedge. *Int. J. Fract. Mech.* **7,** 317–330.

Ojalvo, I. U. and Eidinoff, H. L. (1978). Bond thickness effects upon stresses in single-lap adhesive joints. *AIAA J.* **16,** 204–211.

Oplinger, D. W. (1991). A layered beam theory for single lap joints. Army Materials Technology Laboratory Report MTL TR91-23.

Sneddon, I. (1961). The distribution of stress in adhesive joints. In *Adhesion* (Edited by D. D. Eley), Chapter 9, Oxford University Press.

Tsai, M. Y. and Morton, J. (1992a). On analytical and numerical solutions to the single-lap joint. Center for Adhesive and Sealant Science, VPI, Report CASS/ESM-92-8.

Tsai, M. Y. and Morton, J. (1992b). A stress analysis of a thermally loaded bimaterial interface: a localized hybrid analysis. *Mech. Mater.* **13,** 117–130.

Tsai, M. Y. and Morton, J. (1993). Global and local stress analyses of a short single-lap joint (in press).

Volkersen, O. (1938). Die Niektraftverteiling in Zugbeanspruchten mit Konstanten Laschenquerschritten. *Luftfahrtforschung* **15,** 41–47.

Wang, S. S. and Choi, I. (1982a). Boundary-layer effects in composite laminates: part I—free-edge stress singularities. *J. Appl. Mech.* **49,** 541–548.

Wang, S. S. and Choi, I. (1982b). Boundary-layer effects in composite laminates: part II—free-edge stress solutions and basic characteristics. *J. Appl. Mech.* **49,** 549–560.

Williams, M. L. (1952). Stress singularities resulting from various boundary conditions in angular corners of plates in extension. *J. Appl. Mech.* **19,** 526–528.

Wooley, G. R. and Carver, D. R. (1971). Stress concentration factors for bonded lap joints. *J. Aircraft* **8,** 817–820.

Zienkiewicz, O. C. (1977). *The Finite Element Method.* McGraw-Hill, London.

APPENDICES

In order to provide for convenient comparison with the original treatments, the original notation and definitions are used in these Appendices. These are not, however, totally consistent with those used in the main text.

Appendix A (modified Goland and Reissner's solution)

Goland and Reissner's paper (1944) can be modified to account for the effect of an adhesive layer by rewriting their eqn (7) as:

$$M_1 = T[\alpha_n x_1 - w_1], \qquad 0 \leqslant x_1 \leqslant l$$
$$M_2 = T\left[\alpha_n(l+x_2) - w_2 - \frac{t+\eta}{2}\right], \quad 0 \leqslant x_2 \leqslant c, \tag{A.1}$$

where

$$\alpha_n = \frac{t+\eta}{2(l+c)}.$$

The differential equations for the transverse deflections of the outer adherend and the overlap become:

$$\frac{d^2 w_1}{dx_1^2} = -\frac{M_1}{D_1} = -\frac{T}{D_1}[\alpha_n x_1 - w_1], \qquad 0 \leqslant x_1 \leqslant l$$
$$\frac{d^2 w_2}{dx_2^2} = -\frac{M_2}{D_2} = -\frac{T}{D_2}\left[\alpha_n(l+x_2) - w_2 - \frac{t+\eta}{2}\right], \quad 0 \leqslant x_2 \leqslant c, \tag{A.2}$$

where D_1 and D_2 are the flexural rigidities of the outer adherend and the overlap:

$$D_1 = \frac{Et^3}{12(1-\nu^2)}, \quad D_2 = \frac{2Et^3}{3(1-\nu^2)} + (\tfrac{1}{2}t\eta^2 + t^2\eta)\frac{E}{1-\nu^2} + \frac{E_c\eta^3}{12(1-\nu_c^2)}.$$

The differential equations (A.2) can be solved and the solutions expressed as:

$$w_1 = A_1 \cosh u_1 x_1 + B_1 \sinh u_1 x_1 + \alpha_n x_1, \qquad 0 \leqslant x_1 \leqslant l$$
$$w_2 = A_2 \cosh u_2 x_2 + B_2 \sinh u_2 x_2 + \alpha_n \left(1 + x_2 - \frac{t+\eta}{2\alpha_n}\right), \quad 0 \leqslant x_2 \leqslant c, \tag{A.3}$$

where

$$u_1 = \sqrt{\frac{T}{D_1}} \quad \text{and} \quad u_2 = \sqrt{\frac{T}{D_2}}.$$

The external boundary conditions, which are simple supports at the ends, and the internal boundary conditions, in which the transverse deflections and rotation angles at the ends of the joint overlap should be continuous and the deflection at the anti-symmetric point zero, are:

$$w_1(0) = w_2(c) = 0$$
$$w_1(l) = w_2(0)$$
$$\frac{dw_1}{dx_1} = \frac{dw_2}{dx_2}, \quad \text{for} \quad x_1 = l,\ x_2 = 0. \tag{A.4}$$

The eqns (A.3) associated with the boundary conditions, eqns (A.4), can be solved and the main constant coefficients, A_1 and B_1 become:

$$A_1 = 0,$$
$$B_1 = -\frac{u_2(t+\eta)}{2} \frac{\cosh u_2 c}{u_2 \sinh u_1 l \cosh u_2 c + u_1 \cosh u_1 l \sinh u_2 c}. \tag{A.5}$$

From eqn (A.3), the deflection w_1 can be written as:

$$w_1 = B_1 \sinh u_1 x_1 + \alpha_n x_1. \tag{A.6}$$

The joint edge moment, M_o (at $x_1 = l$) can be derived from eqn (A.2) and eqn (A.6) in terms of loading, geometric, and material parameters:

$$M_o = (M_1)_{x_1 = l} = -D_1 \left(\frac{d^2 w_1}{dx_1^2}\right)_{x_1 = l} = T(\alpha_n l - (w_1)_{x_1 = l})$$
$$= -TB_1 \sinh u_1 l = \frac{T(t+\eta)}{2} \left(\frac{u_2 \cosh u_2 c \sinh u_1 l}{u_2 \sinh u_1 l \cosh u_2 c + u_1 \cosh u_1 l \sinh u_2 c}\right). \tag{A.7}$$

Then, the joint edge moment can be normalized by $Tt/2$ and rewritten as a new factor, k:

$$k = \frac{M_o}{(Tt/2)} = \frac{(t+\eta)}{t} \left(\frac{u_2 \cosh u_2 c \sinh u_1 l}{u_2 \sinh u_1 l \cosh u_2 c + u_1 \cosh u_1 l \sinh u_2 c}\right). \tag{A.8}$$

If the value of $u_1 l$ is sufficiently large to take an approximation as:

$$\sinh u_1 l \approx \cosh u_1 l \approx \tfrac{1}{2} e^{u_1 l}, \tag{A.9}$$

k is reduced to:

$$k = \frac{(t+\eta)}{t} \left(\frac{u_2 \cosh u_2 c}{u_2 \cosh u_2 c + u_1 \sinh u_2 c}\right). \tag{A.10}$$

Appendix B (the corrected Oplinger solution)

The governing equations (21.1), (21.2) and (21.3), shown in Oplinger's paper (1991) are:
for the displacement in the outer adherend

$$\frac{d^2 w_u}{dx^2} - \frac{U^2}{t^2} w_u = \frac{U^2}{t^2} \alpha x, \tag{B.1}$$

for the displacement in the overlap

$$\frac{d^2 \bar{w}}{dx^2} - \frac{U^2}{8t^2} \bar{w} = \frac{U^2}{8t^2} \left(\alpha x - \frac{t+t_b}{2}\right) + \frac{t+t_b}{2} \frac{1}{D_u} \delta_t, \tag{B.2}$$

and for the resultant difference in the overlap

$$\frac{d^2\delta_T}{dx^2} - 2\frac{\beta^2}{t^2}\delta_T = 2G_b\frac{t}{t_b}\frac{d^2\bar{w}}{dx^2}. \tag{B.3}$$

The equation (B.2) is, however, incorrect and should be:

$$\frac{d^2\bar{w}}{dx^2} - \frac{U^2}{2t^2}\bar{w} = \frac{U^2}{2t^2}\left(\alpha x - \frac{t+t_b}{2}\right) + \frac{t+t_b}{4}\frac{1}{D_u}\delta_T. \tag{B.4}$$

Therefore, the homogeneous parts of eqns (B.3) and (B.4) become:

$$\bar{w}_h'' - \frac{U^2}{2t^2}\bar{w}_h + \frac{t+t_b}{4D_u}\delta_{Th} = 0, \tag{B.5}$$

and

$$\delta_{Th}'' - \frac{2\beta^2}{t^2}\delta_{Th} - 2\beta^2 E'\bar{w}_h'' = 0 \tag{B.6}$$

which correspond to eqns (22.1) and (22.2) in Oplinger's paper.

Then, the complete solutions of eqns (B.3) and (B.4) can be written as

$$\bar{w} = \frac{t}{2}k_{21}\frac{\sinh[\mu_1(x-L)/t]}{\sinh(\mu_1\lambda/2)} + \frac{t}{2}k_{22}\frac{\sinh[\mu_2(x-L)/t]}{\sinh(\mu_2\lambda/2)} + \frac{t+t_b}{2} - \alpha x, \tag{B.7}$$

and

$$\delta_T = \Delta_{h1}\frac{\sinh[\mu_1(x-L)/t]}{\sinh(\mu_1\lambda/2)} + \Delta_{h2}\frac{\sinh[\mu_2(x-L)/t]}{\sinh(\mu_2\lambda/2)}. \tag{B.8}$$

Finally, the expression for k can be reduced to:

$$k = \frac{R_1\left(1+\frac{t_b}{t}+R^2C_2\right) + 8R_2\frac{T_{h21}}{T_{h22}}R\left[C_1\left(1+\frac{t_b}{t}\right)-C_2\right]}{R_1 + 8R_2\frac{T_{h21}}{T_{h22}}RC_1 + \sqrt{8}(1+R^2C_1)\frac{T_{h21}}{T_{h1}}}, \tag{B.9}$$

which represents the corrected form of eqn (47) in Oplinger's paper.